Silicon-charge-pump operation limit above and below liquid-helium temperature

Ajit Dash,[1,*] Steve Yianni,[1,2] MengKe Feng,[1,2] Fay Hudson,[1,2] Andre Saraiva,[1,2] Andrew S. Dzurak,[1,2] and Tuomo Tanttu[1,2,†]

[1] *School of Electrical Engineering and Telecommunications, University of New South Wales, Sydney, New South Wales 2052, Australia*

[2] *Diraq, Sydney, New South Wales 2052, Australia*

(Received 29 September 2023; revised 6 December 2023; accepted 19 December 2023; published 22 January 2024)

Semiconductor tunable-barrier single-electron pumps can produce output current of hundreds of picoamperes at sub-parts-per-million precision, approaching the metrological requirement for the direct implementation of the current standard. Here we operate a silicon metal-oxide-semiconductor electron pump up to a temperature of 14 K to qualitatively understand the effect of temperature on charge-pumping accuracy. The uncertainty of the charge pump is tunnel limited below liquid-helium temperature, implying lowering the temperature further does not greatly suppress errors. Hence, highly accurate charge pumps could be achieved in a ^{4}He cryogenic system, further promoting use of the revised quantum current standard across national measurement institutes and industries worldwide.

DOI: 10.1103/PhysRevApplied.21.014040

I. INTRODUCTION

The seven base units of the International Systems of Units (SI) serve as the basis for measuring any physical quantity. Redefining these units over the years aims to ascertain a consistent and universal metrological standard. Recent revision of the SI suggests the use of a quantized charge pump for the practical realization of the primary current standard, by agreeing a fixed value of the elementary charge e $(= 1.602176634 \times 10^{-19}$ A s) [1,2]. A charge pump is a nanoelectronic device that transfers integer-n electrons, holes, or Cooper pairs per voltage cycle with frequency f, yielding quantized current I $(= n \times e \times f)$. A clock-controlled on-demand charge-emitting characteristic of a charge pump is also attracting attention in the fields of quantum information processing and quantum optics [3,4]. Significant research has been pursued by national measurement institutes and academia to realize quantized pumping of quasiparticles in variety of metal, superconductor, metal-superconductor-hybrid, and semiconductor systems [5,6].

Silicon-metal-oxide-semiconductor- (SiMOS) nanostructure-based charge pumps have evinced the potential of practical realization of the SI ampere by demonstrating a remarkable combination of pumping speed and fidelity [7–13]. Besides, quantum devices fabricated on Si have exhibited significant reduction of $1/f$ noise and background charge fluctuations in regimes of high-amplitude operation [14,15]. SiMOS gate-stack technology enables fabrication of multilayer top gates, facilitating strong planar electrostatic confinement to define a quantum dot (QD) [16]. Owing to the small physical size, the electronically defined QD in Si has high charging energy, and hence is capable of transferring a discrete number of charges at a base temperature of the sample space (T_{base}) up to a few kelvins [8,10–12,17]. The influence of temperature on the charge-pumping accuracy has not been assessed in any physical system. Understanding the temperature limit is crucial to choose an optimal T_{base}, which might further relax the requirement of ^{3}He or a dilution refrigerator. In addition to the temperature of the sample space, ac-periodic-drive-induced heating also accounts for an increase in local electron temperature, which may degrade the charge-pumping accuracy [18]. Therefore, in this work we perform a qualitative analysis to understand the impact of sample-space temperature on the charge-pumping accuracy for a wide range of pulsing drive amplitudes. We realize quantized electron pumping using a normal-accuracy-measurement setup [16] in a voltage-induced Si QD up to T_{base} of 14 K by varying the pulsing drive amplitude between 300 and 650 mV. We fit the measured current plateaus to nonequilibrium decay-cascade and equilibrium thermal models of charge transfer to quantify the charge-capturing mechanism as a function of T_{base} and pulsing drive amplitude. We find that the transition temperature [18] between the tunnel-limited electron-capture mechanism and the thermally limited electron-capture mechanism in our Si-based charge pump is higher than the liquid-helium temperature (approximately 4.2 K) for the

*ajit.dash@unsw.edu.au
†t.tanttu@unsw.edu.au

wide range of pulsing drive amplitudes while pumping a single electron per voltage cycle of 100-MHz frequency. Later, these results forecast the lower bound of theoretical errors of the charge pump when it is operated above and below the transition temperature. In our experiments, the precision of the charge-pumping plateaus is limited by the noise level of the room-temperature transimpedance amplifier used for preamplification of the output current. This may lead to overestimation of the uncertainty figure compared with the charge-pump capability. However, the conclusion of this work is not dependent on the accurate value of measurement errors in the charge-pumping plateaus.

II. METHODS

The charge pump measured in this work is fabricated on a near-intrinsic silicon substrate with a 7-nm-thick thermally grown silicon dioxide (SiO_2) layer. The aluminum (Al) gate-stack architecture in Figs. 1(a) and 1(b) is realized by defining the device morphology with electron-beam lithography, followed by thermal evaporation of the subsequent three Al metal layers. Al top gates are electrically insulated from the adjoining metal gates by thermally growing aluminum oxide (Al_xO_y) of 3-nm thickness between each layer. Top gates are connected to a programmable room-temperature dc bias source through a 300-MHz cryogenic low-pass filter. A QD is electrically induced under the plunger lead (PL) by tuning the planar confinement potentials (V_{C1} and V_{C2}) and tunneling-barrier potentials (V_{BL} and V_{BR}). Clock-controlled charge-transfer characteristics of the pump are instigated by adding an ac sine waveform with a time period of 10 ns, generated with use of an arbitrary-waveform generator connected to the BL pulsing barrier gate in Fig. 1(a). The periodic drive modulates the BL barrier potential as shown in Fig. 1(b) to load an electron from the source reservoir [(i) in Fig. 1(b)], followed by capture of the electron in the QD [(ii) in Fig. 1(b)] and finally unloading of it to drain reservoir [(iii) in Fig. 1(b)], generating a pump current (I). The output current is preamplified with a gain of 10^8 V/A with use of a transimpedance amplifier and is measured with a voltmeter by integration over a time of 20 ms, or one power-line cycle. The pumped current is normalized as I/ef to elucidate the average number of electrons pumped per ac voltage cycle $\langle n \rangle$. All the measurements are performed in a variable-temperature insert at T_{base} ranging from 2 to 14 K with a cryogenic temperature controller. A single sweep

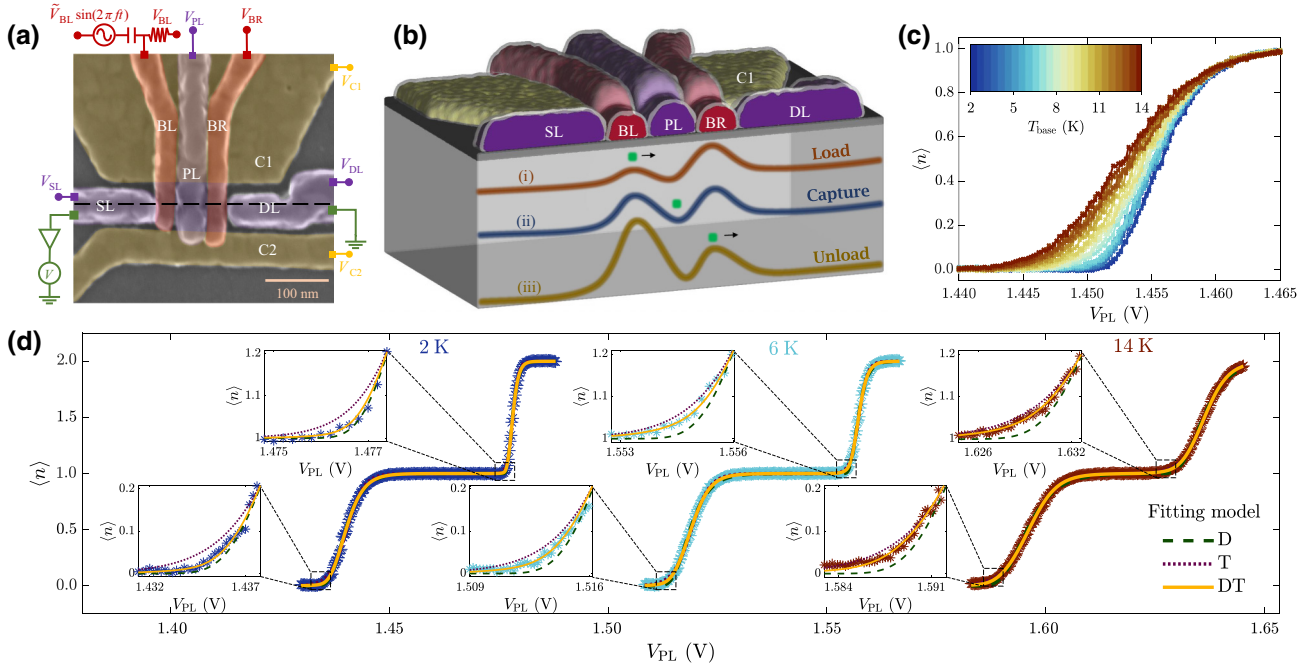

FIG. 1. (a) False-color scanning-electron micrograph of an electron pump similar to one used in the experiment together with a schematic of the measurement setup. (b) Three-dimensional cross-section schematic of the charge pump along the dashed black line in (a) showing the three-layer (yellow, 20 nm; red, 27 nm; violet, 35 nm) gate-stack architecture. (i) Load, (ii) capture, and (iii) unload illustrate the conduction-band-energy-level profile during three stages of an electron (green dot) pumping cycle. (c) Average number of pumped electrons per ac voltage cycle $\langle n \rangle$ as a function of plunger lead voltage V_{PL} with varying base temperature of the sample space (T_{base}) up to 14 K. (d) Plateaus of measured $\langle n \rangle$ at T_{base} of 2, 6, and 14 K along with the fit to the decay-cascade model (D), the thermal model (T), and a weighed sum of the decay-cascade model and the thermal model (DT) of charge pumping. The insets show enlarged axes at the rising edge of the first and second plateaus. The data are horizontally shifted for clarity.

of the measured T_{base}-dependent normalized pump current as a function of the plunger lead voltage V_{PL} at a constant ac-periodic-drive amplitude $\widetilde{V}_{\text{BL}}$ of 350 mV is displayed in Fig. 1(c).

III. RESULTS

We observe a smooth rise to the $\langle n \rangle$ plateau with increasing T_{base} from 2 to 14 K; see Fig. 1(c). This corroborates the occurrence of dissimilar electron-transfer mechanisms in our charge pump, which is explained by decay-cascade [19] and thermal [7,20] models by elaboration of the process of periodic decoupling of the QD from the source-reservoir lead. The decay-cascade model assumes that the dominant charge-pumping-error mechanism is a series of nonequilibrium electron-escape events back to the source reservoir to yield $\langle n_{\text{D}} \rangle$ trapped electrons in the QD, given as

$$\langle n_{\text{D}} \rangle = \sum_{i=1}^{2} \exp\{-\exp[\alpha^*_{\text{D}_i}(V_{\text{PL}} - V_{0_i,\text{D}})]\}, \qquad (1)$$

where α^*_{D} is the gate-referred tunneling rate factor and $V_{0,\text{D}}$ is the threshold voltage obtained from the decay-cascade fit of the normalized pump current. The double-exponential function describing the decay-cascade regime in Eq. (1) analytically has an asymmetric rise shape.

At elevated temperatures, the broader energy spectrum of the electron reservoir becomes the dominating error process, to capture $\langle n_{\text{T}} \rangle$ electrons in the QD [7]. The average number of electrons pumped in the thermal regime is ascertained by the Fermi distribution of electrons in the source-reservoir leads at thermal equilibrium, expressed as

$$\langle n_{\text{T}} \rangle = \sum_{i=1}^{2} 1/\{1 + \exp[\beta^*_{\text{T}_i}(V_{\text{PL}} - V_{0_i,\text{T}})]\}, \qquad (2)$$

where β^*_{T} is the gate-referred modified thermodynamic β and $V_{0,\text{T}}$ is the threshold voltage obtained from the thermal fit of the normalized pump current, which analytically has a symmetric rise shape. The phenomenological fit parameter β^*_{T} corresponds to heat induced by the ac periodic drive, required to cause the charge-pumping process, and inferred as $\beta^*_{\text{T}} = (e\alpha_{\text{PL-QD}})/(k_B T_{\text{pump}})$, where $\alpha_{\text{PL-QD}}$ is the lever arm of PL to the pump QD and T_{pump} is the fitted electron temperature at the source-reservoir and drain-reservoir leads. We calculate $\alpha_{\text{PL-QD}} = e(\Delta V_{\text{SD}}/\Delta V_{\text{PL}})$ from the slope of experimentally measured V_{PL} versus V_{SD} when an electron is added to the QD from the source reservoir.

To have better understanding of the breakdown of tunnel-limited and thermally limited errors, we simply combine the decay-cascade and thermal-charge-capturing models with an error weight, referred as "combined model," given as

$$\langle n_{\text{DT}} \rangle = \sum_{i=1}^{2} (\zeta_{\text{DT}_i}) \times \exp\{-\exp[\alpha^*_{\text{DT}_i}(V_{\text{PL}} - V_{0_i,\text{DT}_\text{D}})]\} + (1 - \zeta_{\text{DT}_i}) \times 1/\{1 + \exp[\beta^*_{\text{DT}_i}(V_{\text{PL}} - V_{0_i,\text{DT}_\text{T}})]\}, \qquad (3)$$

where ζ_{DT} is the weight of the nonequilibrium decay-cascade component in the combined model, having statistical bounds of the confidence interval between 0 and 1, α^*_{DT} is the temperature-independent gate-referred tunneling rate factor obtained from the decay-cascade fit, $1 - \zeta_{\text{DT}}$ is the weight of the equilibrium thermal component in the combined model, β^*_{DT} is the gate-referred modified thermodynamic β of the thermal component in the combined model, and V_{0,DT_D} and V_{0,DT_T} are the threshold voltages of the decay-cascade and thermal components in the combined model, respectively.

To investigate the dependency of temperature on the charge-pumping mechanism, we fit $\langle n \rangle$ associated with the one-electron-pumping and two-electron-pumping plateaus, measured as a function of V_{PL} at varied T_{base}, while keeping the top-gate dc voltages constant at $V_{\text{BL}} = 1.20$ V, $V_{\text{BR}} = 2.28$ V, $V_{\text{SL}} = 2.2$ V, $V_{\text{DL}} = 2.2$ V, $V_{\text{C1}} = 0$ V, and $V_{\text{C2}} = 0$ V. The fitting of the measured data to the aforementioned decay-cascade model [Eq. (1)], thermal model [Eq. (2)] and combined model [Eq. (3)] is shown in Fig. 1(d). The magnified axes in the insets in Fig. 1(d) visibly show that the decay-cascade model fits better at lower T_{base}. However, with increase of T_{base}, the measured plateaus start agreeing more with the thermal model. To quantify the electron-transfer mechanism as a function of T_{base}, we use two approaches. First, we individually determine the average residual sum of squares (RSS) of the decay-cascade fit ($\mu_{\text{RSS,D}}$) and the thermal fit ($\mu_{\text{RSS,T}}$) to the experimental data. A statistical value of $\Delta\mu_{\text{RSS}}$ ($= \mu_{\text{RSS,D}} - \mu_{\text{RSS,T}}$) less than zero implies a better fit to the decay-cascade model, whereas a positive $\Delta\mu_{\text{RSS}}$ indicates the better fit of the thermal model; see Fig. 2(a). Second, we benchmark the weight component of ζ_{DT} at 0.5, signifying the transition from the regions where the decay-cascade model or the thermal model fits better; see Fig. 2(b). The operating regime of the charge pump is purely decay cascade if ζ_{DT} is about unity; in contrast, ζ_{DT} close to zero corresponds to the thermal mechanism of electron capture in the QD. From the results in Figs. 2(a) and 2(b), we find our charge pump operates in the decay-cascade regime at T_{base} less than 5 K while transferring a single electron per voltage cycle. However, pumping two electrons shifts this decay cascade to a thermal transition below a temperature of 4 K.

The phenomenological fit parameter α^*_{D} is related to the tunneling rate of excess electrons ($\Gamma^{\text{escape}}_{\text{D}_i}$), escaping back to the source reservoir, leaving $\langle n \rangle$ electrons in the

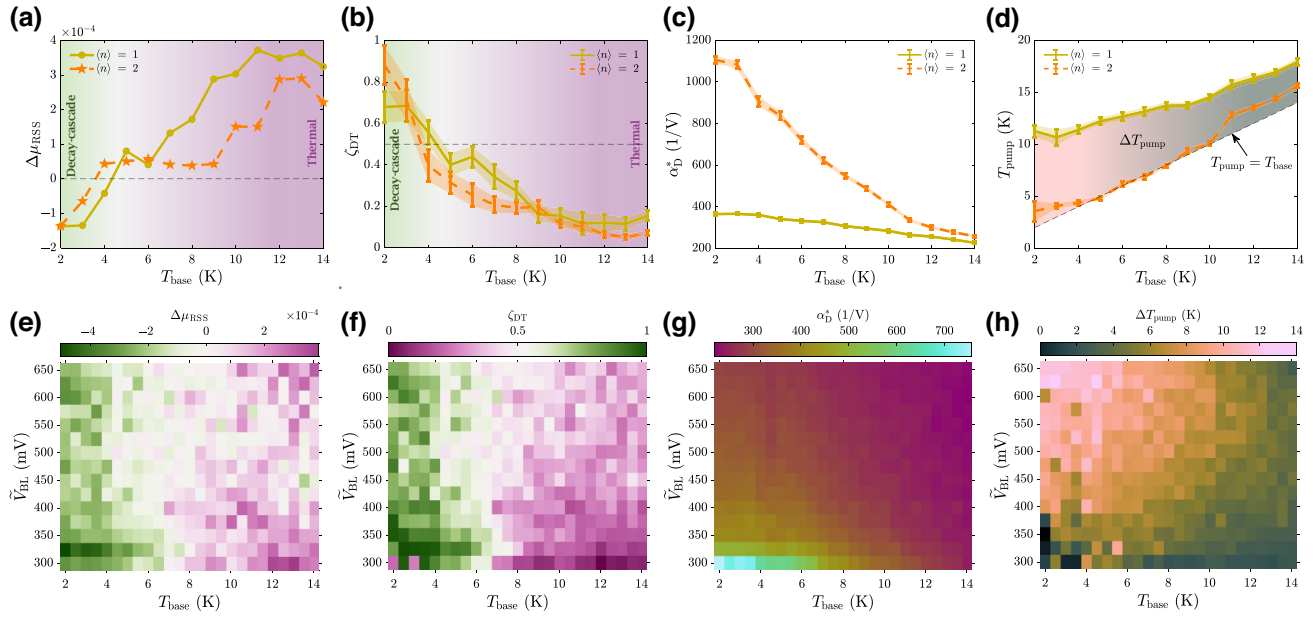

FIG. 2. Phenomenological fitting parameters along with error bars, extracted from the decay-cascade model (D), the thermal model (T), and a weighed sum of the decay-cascade model and the thermal model (DT) of charge pumping for the first and second plateaus as a function of the base temperature of the sample space (T_{base}). (a) Difference between the average residual sum of squares of the decay-cascade and thermal fits of the measured data ($\Delta\mu_{\text{RSS}}$). (b) Weight component of decay-cascade (ζ_{DT}) and thermal ($1-\zeta_{\text{DT}}$) in the combined model. (c) Gate-referred tunneling rate factor (α_{D}^{*}). (d) Fitted electron temperature at the source-reservoir and drain-reservoir leads (T_{pump}). The difference between the dashed black line (at T_{base}) and T_{pump} depicts the ac-periodic-drive-induced heating in the pump (ΔT_{pump}). (e) $\Delta\mu_{\text{RSS}}$, (f) ζ_{DT}, (g) α_{D}^{*}, and (h) ΔT_{pump} for single-electron pumping, measured as a function of T_{base} and drive amplitude ($\widetilde{V}_{\text{BL}}$).

QD. One can theoretically forecast the lower bound of uncertainties encountered during the process of pumping from the difference $(\alpha_{\text{D}_2}^{*}V_{0_2,\text{D}})-(\alpha_{\text{D}_1}^{*}V_{0_1,\text{D}})$, which is equivalent to the difference in the back-tunneling rate of excess electrons $\ln\Gamma_{\text{D}_2}^{\text{escape}}-\ln\Gamma_{\text{D}_1}^{\text{escape}}$ [18,19]. Although α_{D}^{*} is independent of temperature, the regression-analysis results reveal a decrease in $\alpha_{\text{D}_1}^{*}$ and $\alpha_{\text{D}_2}^{*}$ when the charge pump is operated in the thermal regime, corresponding to T_{base} higher than the transition temperature. In contrast, we observe saturation of α_{D}^{*} for both one-electron transfer and two-electron transfer when T_{base} is lower than the transition temperature; see Fig. 2(c).

Although the charge pump is cooled to T_{base}, T_{pump} may be higher due to ac-periodic-drive-induced heating [7,18]. To assess T_{pump} while we pump one electron and two electrons per voltage cycle, we use the gate-referred modified thermodynamic β extracted from the thermal component of the combined model to evaluate the value of $T_{\text{pump}_i}=(e\alpha_{\text{PL-QD}})/(k_B\beta_{\text{DT}_i}^{*})$. For a fair comparison of the ac-periodic-drive-induced electron temperature at the source reservoir as a function of T_{base}, we evaluate the heat induced in the pump $\Delta T_{\text{pump}}=T_{\text{pump}}-T_{\text{base}}$; see Fig. 2(d). We find that the heat induced by the ac periodic drive in our system is higher during transfer of a single electron per cycle than during transfer of two electrons per cycle. However, the number of electrons existing in the QD before initialization of the charge-pumping process might have an influence on the value of ΔT_{pump}. Therefore, the gate-referred modified thermodynamic β used to deduce T_{pump} for the two-electron plateau deserves further theoretical and experimental investigation.

Next, we turn our attention to the impact of $\widetilde{V}_{\text{BL}}$ on the single-electron-pumping fit parameters ($\Delta\mu_{\text{RSS}}$, ζ_{DT}, α_{D}^{*}, and ΔT_{pump}) as a function of T_{base} and $\widetilde{V}_{\text{BL}}$. The top-gate dc voltages are kept constant at $V_{\text{BL}}=1.32$ V, $V_{\text{BR}}=2.38$ V, $V_{\text{SL}}=2.2$ V, $V_{\text{DL}}=2.2$ V, $V_{\text{C1}}=-0.03$ V, and $V_{\text{C2}}=0$ V and we perform measurements for different values of $\widetilde{V}_{\text{BL}}$ and T_{base}. $\Delta\mu_{\text{RSS}}$ and ζ_{DT} in Figs. 2(e) and 2(f), respectively, reveal a leftward shift of the transition temperature with rising $\widetilde{V}_{\text{BL}}$. In addition, it is worth noting that α_{D}^{*} decreases with an increase in $\widetilde{V}_{\text{BL}}$ in Fig. 2(g). This informs us of the importance of tuning the $\widetilde{V}_{\text{BL}}$ amplitude. Further, the evaluated value of ΔT_{pump} supports the statement that at a particular T_{base} the heat induced is directly proportional to $\widetilde{V}_{\text{BL}}$; see Fig. 2(h).

For a qualitative investigation of the single-electron-pumping uncertainties, we follow a theoretical approach to assess the lower bound of error occurring during the single-electron-pumping processes [19]. To determine the charge-pumping error (ϵ_{pump}) as a function of $\widetilde{V}_{\text{BL}}$ and T_{base}, we use the single-electron-transfer experimental data, which are measured as a function of V_{PL} by varying $\widetilde{V}_{\text{BL}}$ and

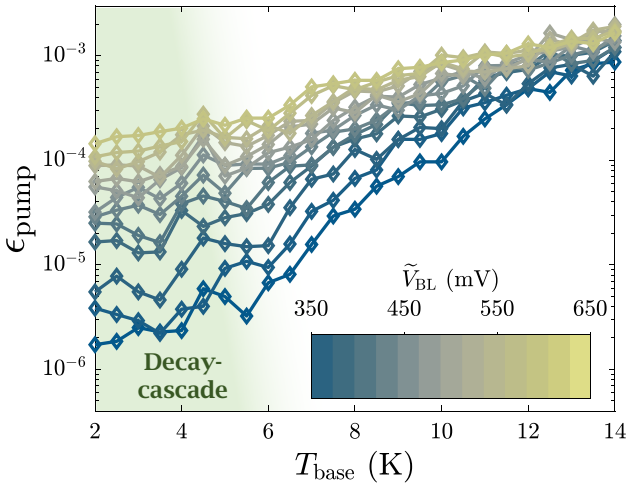

FIG. 3. Lower bound of single-electron-pumping error (ϵ_{pump}) as a function of drive amplitude ($\widetilde{V}_{\mathrm{BL}}$) and base temperature of the sample space (T_{base}).

T_{base}, a single sweep of which (at $\widetilde{V}_{\mathrm{BL}} = 400$ mV) is shown in Fig. 1(c). ϵ_{pump} is given as $1 - \langle n_{\mathrm{D}} \rangle$ at the point of inflection (V^*_{PL}) on the $\langle n \rangle = 1$ plateau. When calculating ϵ_{pump}, we assume that $\alpha^*_{\mathrm{D}_1} = \alpha^*_{\mathrm{D}_2}$ and that $\Delta V_{0,\mathrm{D}} (= V_{0_2,\mathrm{D}} - V_{0_1,\mathrm{D}})$ is independent of $\widetilde{V}_{\mathrm{BL}}$. The lower bound of the evaluated single-electron-pumping error as a function of T_{base} and $\widetilde{V}_{\mathrm{BL}}$ is illustrated in Fig. 3. The theoretical error rate of our Si single-electron pump when operated at $T_{\mathrm{base}} = 2$ K and $\widetilde{V}_{\mathrm{BL}} = 350$ mV is 1.72 ppm. At constant T_{base}, the reduction in $\widetilde{V}_{\mathrm{BL}}$ leads to sharper edges of the plateau, and theoretically a lower error bound. Besides, the results show that single-electron-pumping error is almost independent of T_{base} for operation in a regime where an electron is captured in the pump QD by following a sequence of tunneling events back to the source reservoir.

IV. SUMMARY

Overall, we show that our Si single-electron pump is operable at liquid-helium temperature with tunnel-limited errors dominating the pump fidelity, indicating high-precision metrological current measurements could be consistently performed in cheap ^{4}He systems. This paves the way for a transportable and scalable primary SI current standard by use of SiMOS technology, which is well-established across semiconductor foundries. Although the results of the experiment do not show the universality of the transition temperature, it is likely to be above or around the liquid-helium temperature for SiMOS devices with the same architecture. Showing the universality of the transition temperature will require more device statistics. To further assess the charge-pump fidelity, an on-chip charge sensor could be used to detect the error events [21].

ACKNOWLEDGMENTS

We thank M. Mamunur Rahman and Alexandra Dickie for assistance with the cryogenic setup. We acknowledge support from the Australian Research Council (DP200103515), the U.S. Army Research Office (Grant No. W911NF-17-1-0198), and the New South Wales node of the Australian National Fabrication Facility. A.D. and M.F. acknowledge scholarship support from the Sydney Quantum Academy, Australia.

A.D. performed all measurements and all calculations under T.T.'s supervision. S.Y. and F.H. fabricated the device under A.S.D.'s supervision. A.D., S.Y., M.K.F., A.S., and T.T. participated in data interpretation. A.D., S.Y., and T.T. designed the project and the experimental setup. A.D. wrote the manuscript with contributions from all authors.

[1] P. J. Mohr, D. B. Newell, B. N. Taylor, and E. Tiesinga, Data and analysis for the CODATA 2017 special fundamental constants adjustment, Metrologia **55**, 125 (2018).

[2] A. Rossi, N. W. Hendrickx, A. Sammak, M. Veldhorst, G. Scappucci, and M. Kataoka, Single-hole pump in germanium, J. Phys. D: Appl. Phys. **54**, 434001 (2021).

[3] N. Johnson, C. Emary, S. Ryu, H.-S. Sim, P. See, J. Fletcher, J. Griffiths, G. Jones, I. Farrer, D. Ritchie, M. Pepper, T. J. B. M. Janssen, and M. Kataoka, LO-phonon emission rate of hot electrons from an on-demand single-electron source in a GaAs/AlGaAs heterostructure, Phys. Rev. Lett. **121**, 137703 (2018).

[4] G. Yamahata, S. Ryu, N. Johnson, H.-S. Sim, A. Fujiwara, and M. Kataoka, Picosecond coherent electron motion in a silicon single-electron source, Nat. Nanotechnol. **14**, 1019 (2019).

[5] F. Stein, H. Scherer, T. Gerster, R. Behr, M. Götz, E. Pesel, C. Leicht, N. Ubbelohde, T. Weimann, K. Pierz, H. W. Schumacher, and F. Hohls, Robustness of single-electron pumps at sub-ppm current accuracy level, Metrologia **54**, S1 (2016).

[6] H. Scherer and H. W. Schumacher, Single-electron pumps and quantum current metrology in the revised SI, Ann. Phys. **531**, 1800371 (2019).

[7] R. Zhao, A. Rossi, S. Giblin, J. Fletcher, F. Hudson, M. Möttönen, M. Kataoka, and A. Dzurak, Thermal-error regime in high-accuracy gigahertz single-electron pumping, Phys. Rev. Appl. **8**, 044021 (2017).

[8] S. P. Giblin, E. Mykkänen, A. Kemppinen, P. Immonen, A. Manninen, M. Jenei, M. Möttönen, G. Yamahata, A. Fujiwara, and M. Kataoka, Realisation of a quantum current standard at liquid helium temperature with sub-ppm reproducibility, Metrologia **57**, 025013 (2020).

[9] G. Yamahata, S. P. Giblin, M. Kataoka, T. Karasawa, and A. Fujiwara, High-accuracy current generation in the nanoampere regime from a silicon single-trap electron pump, Sci. Rep. **7**, 45137 (2017).

[10] A. Fujiwara, K. Nishiguchi, and Y. Ono, Nanoampere charge pump by single-electron ratchet using silicon

nanowire metal-oxide-semiconductor field-effect transistor, Appl. Phys. Lett. **92**, 042102 (2008).

[11] G. Yamahata, T. Karasawa, and A. Fujiwara, Gigahertz single-hole transfer in Si tunable-barrier pumps, Appl. Phys. Lett. **106**, 023112 (2015).

[12] A. Rossi, J. Klochan, J. Timoshenko, F. E. Hudson, M. Möttönen, S. Rogge, A. S. Dzurak, V. Kashcheyevs, and G. C. Tettamanzi, Gigahertz single-electron pumping mediated by parasitic states, Nano Lett. **18**, 4141 (2018).

[13] S. Giblin, G. Yamahata, A. Fujiwara, and M. Kataoka, Precision measurement of an electron pump at 2 GHz; the frontier of small DC current metrology, Metrologia **60**, 055001 (2023).

[14] P. Koppinen, M. Stewart, and N. M. Zimmerman, Fabrication and electrical characterization of fully CMOS-compatible Si single-electron devices, IEEE Trans. Electron Devices **60**, 78 (2012).

[15] N. M. Zimmerman, W. H. Huber, B. Simonds, E. Hourdakis, A. Fujiwara, Y. Ono, Y. Takahashi, H. Inokawa, M. Furlan, and M. W. Keller, Why the long-term charge offset drift in Si single-electron tunneling transistors is much smaller (better) than in metal-based ones: Two-level fluctuator stability, J. Appl. Phys. **104**, 033710 (2008).

[16] A. Rossi, T. Tanttu, K. Y. Tan, I. Iisakka, R. Zhao, K. W. Chan, G. C. Tettamanzi, S. Rogge, A. S. Dzurak, and M. Mottonen, An accurate single-electron pump based on a highly tunable silicon quantum dot, Nano Lett. **14**, 3405 (2014).

[17] G. Yamahata, S. P. Giblin, M. Kataoka, T. Karasawa, and A. Fujiwara, Gigahertz single-electron pumping in silicon with an accuracy better than 9.2 parts in 10^7, Appl. Phys. Lett. **109**, 013101 (2016).

[18] G. Yamahata, K. Nishiguchi, and A. Fujiwara, Accuracy evaluation and mechanism crossover of single-electron transfer in Si tunable-barrier turnstiles, Phys. Rev. B **89**, 165302 (2014).

[19] V. Kashcheyevs and B. Kaestner, Universal decay cascade model for dynamic quantum dot initialization, Phys. Rev. Lett. **104**, 186805 (2010).

[20] G. Yamahata, K. Nishiguchi, and A. Fujiwara, Accuracy evaluation of single-electron shuttle transfer in Si nanowire metal-oxide-semiconductor field-effect transistors, Appl. Phys. Lett. **98**, 222104 (2011).

[21] A. Dash, S. Yianni, J. Y. Huang, M. Feng, F. Hudson, A. Saraiva, A. Dzurak, and T. Tanttu, in *2023 IEEE International Conference on Quantum Computing and Engineering (QCE)* (IEEE, 2023), Vol. 2, p. 310.